

Layer-Locked Anomalous Valley Hall Effect in Two-Dimensional A-Type Tetragonal Antiferromagnetic Insulator

San-Dong Guo,^{1,*} Wei Xu,² Yang Xue,³ Gangqiang Zhu,⁴ and Yee Sin Ang^{5,†}

¹*School of Electronic Engineering, Xi'an University of Posts and Telecommunications, Xi'an 710121, China*

²*State Key Laboratory of Surface Physics and Key Laboratory of Computational Physical Sciences (MOE), and Department of Physics, Fudan University, Shanghai 200433, China*

³*Department of Physics, East China University of Science and Technology, Shanghai 200237, China*

⁴*School of Physics and Electronic Information, Shaanxi Normal University, Xi'an 716000, Shaanxi, China*

⁵*Science, Mathematics and Technology (SMT) Cluster, Singapore University of Technology and Design, Singapore 487372*

Antiferromagnetic (AFM) spintronics provides a route towards energy-efficient and ultrafast device applications. Achieving anomalous valley Hall effect (AVHE) in AFM monolayers is thus of considerable interest for both fundamental condensed matter physics and device engineering. Here we propose a route to achieve AVHE in A-type AFM insulator composed of vertically-stacked monolayer quantum anomalous Hall insulator (QAHI) with strain and electric field modulations. Uniaxial strain and electric field generate valley polarization and spin splitting, respectively. Using first-principles calculations, Fe₂BrMgP monolayer is predicted to be a prototype A-type AFM hosting *valley-polarized quantum spin Hall insulator* (VQSHI) in which AVHE and quantum spin Hall effect (QSHE) are synergized in a single system. Our findings reveal a route to achieve multiple Hall effects in 2D tetragonal AFM monolayers.

Introduction.— Utilizing valley degree of freedom to encode and process information, characterized as valleytronics, provides remarkable opportunities for developing next-generation minimized devices [1–7]. Valley refers to a local energy minimum/maximum in conduction/valence band, where these energy extremes are robust against phonon and impurity scatterings due to the large separation in the momentum space[1]. Recent proposals of valleytronics are mainly based on time-reversal-connected valleys, where valley polarization is induced by an external field, dynamically or electrostatically [8–13]. Intrinsic valleytronics materials with spontaneous valley polarization are more advantageous in terms of valley robustness, energy efficiency, and simplicity in operation, which are beneficial for practical device applications. Recently, the ferrovalley (FV) semiconductor has been proposed [14], which possesses spontaneous valley polarization induced by the combined effects of magnetic order and spin-orbit coupling (SOC). Valley-dependent Berry curvature in FV materials leads to anomalous valley Hall effect (AVHE). FV materials thus offer an interesting platform to study valley-contrasting transport and Berry physics.

Achieving spontaneous valley polarization typically requires ferromagnetic (FM) system as a basic premise [15]. Compared with ferromagnetism, antiferromagnetic (AFM) materials with zero magnetic moment are inherently robust to external magnetic perturbation, and possess ultrafast dynamics[16, 17], thus offering enormous potential for both valleytronic and spintronic applications. However, spontaneous valley polarization in AFM materials is rarely reported [18–22], and the AVHE in

AFM system is undesirable suppressed [19, 20]. Furthermore, topological states based on valley-polarized quantum anomalous Hall insulator (VQAHI) has been recently proposed, in which valley polarization and quantum anomalous Hall effect (QAHE) are combined in one material. Such system is particularly interesting due to their compatibility with low-power electronics, spintronics, sensing, metrology and quantum information processing applications [23–25]. Several VQAHI systems have been theoretically proposed by constructing complex heterostructure, layer-dependent proximity effects, and accurate regulation of strain and correlation strength [29–43].

It should also be noted that previously reported valley-polarized AFM systems are mostly based on hexagonal symmetric lattice [18–22]. Whether FV can be achieved in AFM system beyond hexagonal lattice symmetry remains an open question thus far. Can AVHE in AFM materials be achieved in system beyond hexagonal lattices? Is it possible to achieve other valley-polarized topological state? Here we propose a way to realize AVHE in an A-type tetragonal AFM insulator composed of vertically-stacked monolayered quantum anomalous Hall insulator (QAHI) under both strain and electric field tuning. A peculiar valley-polarized quantum spin Hall insulator (VQSHI) can be achieved in the proposed systems, which is verified via first-principles in Fe₂BrMgP monolayer as a prototype VQSHI. Our findings open up a previously unexplored concept of VQSHI in which valley-polarization and quantum spin Hall effect (QSHE) are synergized in a single system.

Achieving AVHE in AFM insulators.— Firstly, a two-dimensional (2D) tetragonal FM QAHI is used as the basic building block, which has a layer of magnetic atoms and possesses equivalent valleys along Γ -X and Γ -Y lines in the first Brillouin zone (BZ) due to C_4 rotation

* sandongyuwang@163.com

† yeemin_ang@sutd.edu.sg

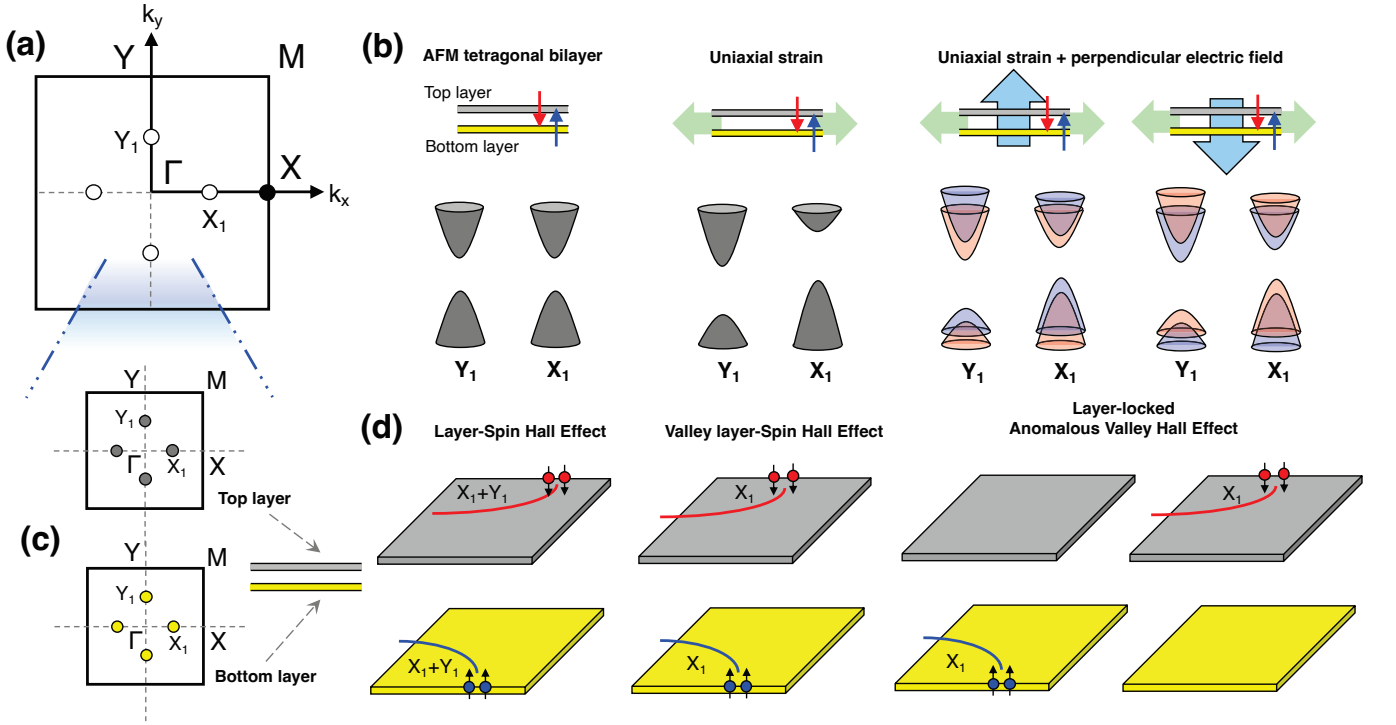


FIG. 1. **Concept of layer-locked anomalous valley Hall effect in 2D tetragonal lattice.** (a) 2D tetragonal lattice possesses equivalent valleys along Γ -X and Γ -Y lines with Berry curvature mainly occurring around Y_1 and X_1 valleys. (b) Applying uniaxial strain along x direction makes the Y_1 and X_1 valleys become unequal but spin degeneracy is still preserved. Simultaneous application of uniaxial strain and out-of-plane electric field further breaks the spin degeneracy. Reversing electric field leads to opposite spin splitting at both Y_1 and X_1 valleys. The spin-up and spin-down channels are depicted in blue and red, respectively. (c): Superposition of two tetragonal QAHIs with equal but opposite magnetic moments (A-type AFM order) leads to spin-degenerate equivalent Y_1 and X_1 valleys with net-zero Berry curvature in momentum space. However, the Berry curvatures for the spin-up and spin-down channels are positive and negative, respectively, yielding nonzero layer-locked hidden Berry curvature in real space. (d) Showing the layer-spin hall effect, valley layer-spin hall effect, and layer-locked anomalous valley Hall effect.

symmetry [Fig.1 (a)]. The Berry curvatures mainly occur around the Y_1 and X_1 valleys with positive values.

To realize AFM insulator, a superposition of two 2D tetragonal FM QAHIs with equal but opposite magnetic moments (A-type AFM order) is constructed [Fig.1 (b)], giving rise to spin degeneracy and equivalent Y_1 and X_1 valleys. Here, we assume that the AFM system has a symmetry of a combination of inversion symmetry \mathcal{P} and time-reversal symmetry \mathcal{T} (\mathcal{PT}), which leads to a spin-degenerate 2D system. To induce valley polarization, a natural way is to destroy C_4 rotation symmetry via uniaxial strain along the x or y direction [Fig.1 (b)]. However, the spin degeneracy is still maintained under uniaxial strain, which prohibits the AVHE. An out-of-plane electric field E_{\perp} is introduced to break the \mathcal{PT} symmetry, which lifts the spin degeneracy of valleys (Fig.1 (b)). Such spin-degeneracy breaking is due to the layer-dependent electrostatic potential $\propto eEd$ (e and d denote the electron charge and the layer distance) created by the out-of-plane electric field, which causes the spin-up and spin-down bands in different layers to stagger, leading to spin-splitting effect. A similar mechanism can be

found in electric potential difference antiferromagnetism [44]. More interestingly, the spin orders at both Y_1 and X_1 valleys can be reversed through reversing the direction of out-of-plane electric field [Fig.1 (b)], thus offering electrostatic field-tunable valley polarization.

The superposition of two tetragonal QAHIs leads to zero Berry curvature $\Omega(k)$ in momentum space due to \mathcal{PT} symmetry [Fig.1 (c)]. However, each layer breaks the \mathcal{PT} symmetry *individually*, which gives rise to the layer-locked *hidden* Berry curvature, and the Berry curvatures for the spin-up and spin-down channels are positive and negative-valued, respectively. Such layer-locked hidden Berry curvature leads to a peculiar layer-Hall effect not commonly found in other AVHE systems.

In the presence of a longitudinal in-plane electric field E_{\parallel} , the Bloch carriers acquire an anomalous transverse velocity $v_{\perp} \sim E_{\parallel} \times \Omega(k)$ [4]. By shifting the Fermi level in the valence band via hole doping, various layer-spin Hall and layer-locked AVHE can occur [Fig.1 (d)]: (i) The spin-up and spin-down electrons from Y_1 and X_1 valleys accumulate along opposite sides of different layers in the case of 2D A-type tetragonal AFM system, result-

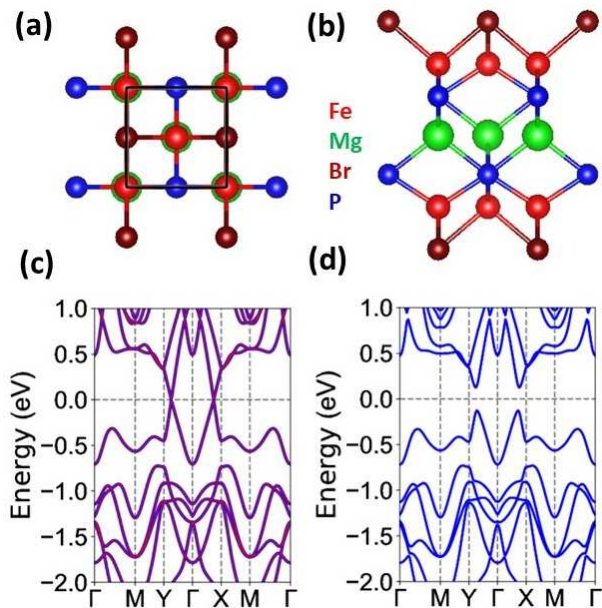


FIG. 2. **Lattice and electronic structures of Fe_2BrMgP monolayer.** (a) and (b): top and side views of monolayer Fe_2BrMgP . Energy band structures of Fe_2BrMgP monolayer (c) without and (d) with SOC. In (c), the spin-up and spin-down channels are depicted in blue and red.

ing in layer-spin hall effect; (ii) when a uniaxial strain is applied, the spin-up and spin-down electrons from only X_1 valley accumulate along the opposite sides of different layers, resulting in valley layer-spin hall effect; (iii) the spin-up/spin-down electrons from only X_1 valley accumulate along one side of bottom/top layer, resulting to the rarely explored *layer-locked anomalous valley Hall effect*.

Material realization.— Monolayer Fe_2XY ($X=\text{or}\neq Y=\text{Cl, Br and I}$) and $\text{Li}_2\text{Fe}_2\text{XY}$ ($X=\text{or}\neq Y=\text{S, Se and Te}$) families[45–50] can be used as the basic building block. These monolayers are tetragonal QAHIs with equivalent valleys along Γ -X and Γ -Y lines in the first Brillouin zone (BZ), and the extremes of Berry curvatures are located at the Y_1 and X_1 valleys. Instead of employing the vertical stacking of two identical monolayers via van der Waals (vdW) heterostructure approach, we consider an intercalation architecture in which two identical monolayers are intercalated to form an ‘ultrathick’ Fe_2XYP monolayer ($X=\text{Br, Cl and I}$; $Y=\text{Mg and Be}$) [51]. We use Fe_2BrMgP as a prototype system to illustrate the concept of layer-locked AVHE in 2D tetragonal AFM. The first-principles calculation details are presented in the Supplementary Materials.

Lattice, magnetic and electronic properties.—

Fe_2BrMgP monolayer is dynamically, mechanically, and thermally stable [51]. The crystal structures of Fe_2BrMgP monolayer are plotted in Fig.2 (a) and (b), crystallizing in the $P4/nmm$ space group (No.129). The unit cell contains ten atoms with seven-atomic layer sequence of Br-Fe-P-Mg-P-Fe-Br. The optimized equi-

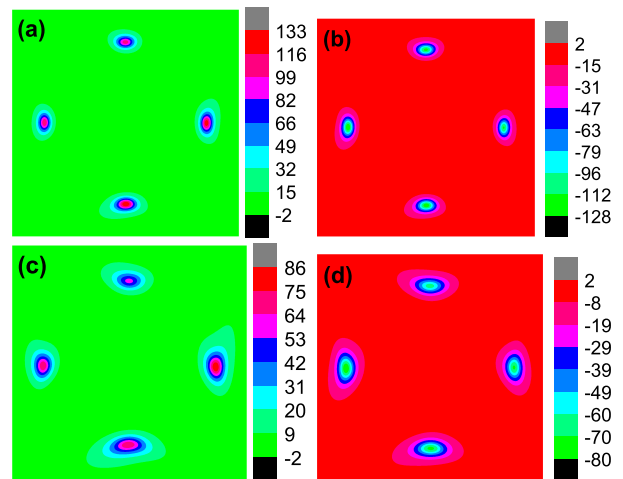


FIG. 3. **Layer-dependent Berry curvature of Fe_2BrMgP .** The Berry curvatures are shown for the spin-up (a,c) and spin-down (b,d) channels for $a/a_0=1.00$ and $E=0.00\text{V}/\text{\AA}$ (a,b), and for $a/a_0=1.04$ and $E=0.02\text{V}/\text{\AA}$ (c,d).

librium lattice constants are $a=b=4.03 \text{\AA}$ by GGA+ U method. To determine the ground state of Fe_2BrMgP , we consider two magnetic configurations, including the intralayer FM and interlayer FM ordering (FM ordering), and intralayer FM and interlayer AFM ordering (A-type AFM ordering). This A-type AFM ordering is predicted to be the ground state, and its energy is 54.86 meV per unit cell lower than that with the FM ordering. The different magnetic orientation can affect the symmetry of a system as well as the valley and topological properties [37–43, 45–50]. For example, in monolayer Fe_2Br_2 , when the magnetic orientation is out-of-plane, the hot spots in the Berry curvature are around four gapped Dirac cone with the same signs, leading to Chern number $C=2$; while for in-plane magnetization, two of four main hot spots in the Berry curvature have the opposite sign with the other two, giving rise to a vanishing Chern number [49]. For our proposed system, an out-of-plane magnetic orientation is needed, and the magnetic orientation can be determined by magnetic anisotropy energy (MAE). By GGA+ U +SOC method, the MAE can be calculated as $E_{MAE} = E_{SOC}^{\parallel} - E_{SOC}^{\perp}$ where \parallel and \perp denotes the in-plane and out-of-plane spin orientation. The MAE is $451\mu\text{eV}/\text{Fe}$, and the positive value indicates the out-of-plane easy magnetization axis of Fe_2BrMgP , which confirms our proposed design principles. The total magnetic moment per unit cell is strictly $0.00 \mu_B$, and the magnetic moments of bottom/top Fe atoms are $3.06 \mu_B/-3.06 \mu_B$.

The calculated energy band structures of Fe_2BrMgP without and with SOC are shown in Fig.2 (c) and (d), respectively. When neglecting SOC, two pairs of band-crossing points occurs near the Fermi level along Γ -X and Γ -Y lines. With SOC, a Dirac gap of 252 meV is introduced, yielding equivalent valleys along the Γ -X and Γ -Y lines due to C_4 rotation symmetry. The corre-

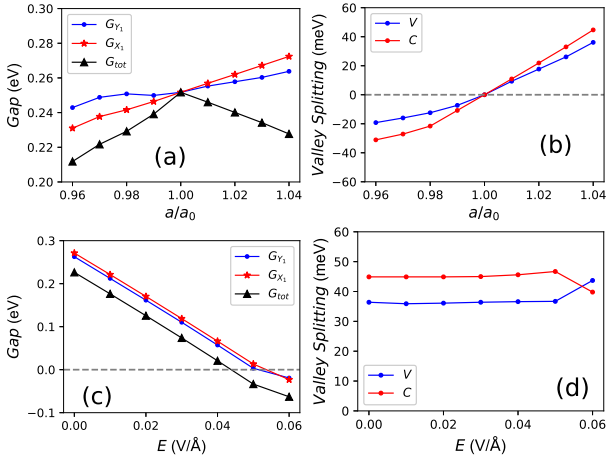


FIG. 4. **Strain and electric field modulation.** For Fe_2BrMgP , the related bandgaps including the global gap [G_{tot}] and gaps of Y_1 and X_1 valleys [G_{Y_1} and G_{X_1}] (a,c) and valley splitting for both valence [V] and condition [C] bands (b,d) as a function of a/a_0 (a,b) and E (c,d) with $a/a_0=1.04$.

sponding k points in the momentum space are marked by X_1 and Y_1 without valley splitting ($\Delta E_C = E_{X_1}^C - E_{Y_1}^C$ and $\Delta E_V = E_{X_1}^V - E_{Y_1}^V$) for both conduction and valence bands. Because of the \mathcal{PT} symmetry, the bands of Fe_2BrMgP are spin degenerate both without and with SOC.

Because of the \mathcal{PT} symmetry, the Berry curvature of Fe_2BrMgP vanishes. However, each layer breaks the \mathcal{PT} symmetry locally, and such layer-specific symmetry breaking leads to a non-vanishing layer-locked hidden Berry curvature. Here the Berry curvatures of spin-up and spin-down channels are non-zero [Fig.3 (a) and (b)]. The Berry curvatures are opposite for spin-up and spin-down channels around Y_1 and X_1 valleys, respectively. In the presence of a longitudinal in-plane electric field E_{\parallel} , the spin-up and spin-down electrons from Y_1 and X_1 valleys will accumulate along opposite sides of the top and bottom Fe layers, resulting in layer-spin hall effect [Fig.1 (d)].

Uniaxial strain induces valley polarization.— To induce valley polarization in Fe_2BrMgP , an uniaxial strain along x or y direction is applied which reduces C_4 to C_2 symmetry. The valleys along the Γ -X and Γ -Y lines become inequivalent, thus giving rise to valley polarization. We use a/a_0 (0.96 to 1.04) to simulate a uniaxial strain along x direction, and the lattice constants b along y direction is optimized. The in-plane Young's modulus $C_{2D}(\theta)$ as a function of the angle θ relative to the x direction is plotted in FIG. S1 of the Supplementary Materials. The obtained C_{2D} along x direction is 86 Nm^{-1} . This is smaller than those of graphene ($\sim 340 \pm 40 \text{ Nm}^{-1}$) and MoS_2 ($\sim 126.2 \text{ Nm}^{-1}$) [52, 53], which indicates the better mechanical flexibility of Fe_2BrMgP , thus favoring the experimental realization of valley polarization by strain. The strained Fe_2BrMgP remains in the

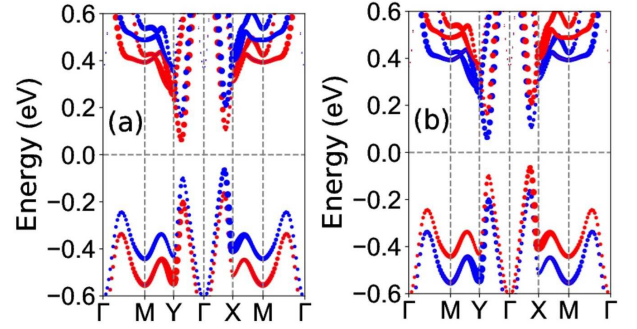


FIG. 5. **Sign-reversible layer-locked anomalous valley Hall effect.** For Fe_2BrMgP with $a/a_0=1.04$, the spin-resolved energy band structures for $E=+0.02\text{V}/\text{\AA}$ (a) and $E=-0.02\text{V}/\text{\AA}$ (b). The spin-up and spin-down channels are depicted in blue and red.

A-type AFM ground state with out-of-plane magnetic anisotropy within the considered strain range (see FIG. S2 of the Supplementary Materials).

The electronic band structures of strained Fe_2BrMgP calculated using GGA+SOC are plotted in FIG. S3 of the Supplementary Materials. The evolution of the bandgap and the valley splitting (ΔE_V and ΔE_C) for both valence and conduction bands as a function of a/a_0 are plotted in Fig.4 (a) and (b). The uniaxial strain induces valley polarization for both conduction and valence bands, and the valley polarization can be switched between X_1 and Y_1 valleys with strain transiting from compressive to tensile cases. For common hexagonal FV systems, the valley polarization can be reversed by magnetic field [37–42]. Therefore, the uniaxial strain can be regarded as a pseudo-magnetic field for tetragonal system [43]. For $a/a_0=0.96/1.04$, the corresponding valley splitting are -19 (-31) $\text{meV}/36$ (45) meV for valence (conduction) band, which are close to or larger than the thermal energy of room temperature (25 meV). Using $a/a_0=1.04$ as a representative, the Berry curvatures of the spin-up and spin-down channels are plotted in FIG. S4 of the Supplementary Materials. The Berry curvatures are opposite for spin-up and spin-down channels around Y_1 and X_1 valleys. In this case, a longitudinal in-plane electric field E_{\parallel} can thus lead to the accumulation of the spin-up and spin-down electrons from only X_1 valleys along the opposite sides of top and bottom Fe layers, resulting in valley layer-spin hall effect as illustrated in Fig.1(d).

Electric field induces spin splitting.— An out-of-plane electric field can break the \mathcal{PT} symmetry to lift the spin degeneracy of the valleys. Taking strained Fe_2BrMgP with $a/a_0=1.04$ as an example, the electric field (E) effects on the electronic structures are investigated. The difference between $+E$ and $-E$ is that the spin-splitting order is reversed. According to FIG. S5 of the Supplementary Materials, the ground state of Fe_2BrMgP remains in the A-type AFM ordering with out-of-plane magnetic anisotropy within the considered E range. The energy band structures of Fe_2BrMgP by using

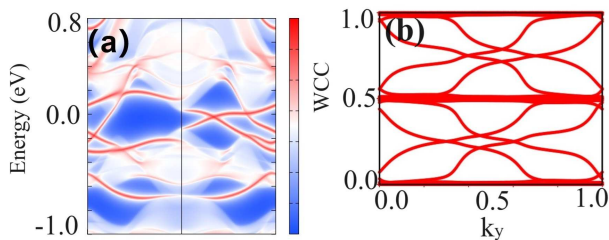


FIG. 6. **Topological properties of Fe₂BrMgP.** For Fe₂BrMgP with $a/a_0=1.04$ at $E=+0.02\text{V}/\text{\AA}$: (a) the edge states along the [100] direction; (b) the evolution of WCCs along k_y .

GGA+SOC at representative E are plotted in FIG. S6 of the Supplementary Materials, and the spin-resolved energy band structures at $E=\pm 0.02\text{V}/\text{\AA}$ are shown in Fig.5. The evolutions of related energy band gap and the valley splitting for both valence and conduction bands as a function of E are plotted in Fig.4 (c) and (d).

The spin splitting induced by out-of-plane electric field, and spin-polarization reversal via reversing the direction of electric field can be observed in Fig.5. The electric field can maintain valley splitting amplitude, and induce a semiconductor-metal phase transition (see Fig.4 (c) and (d)). The sizes of spin splitting at X_1 and Y_1 valleys for both conduction and valence bands are plotted in FIG. S7 of the Supplementary Materials, which meets the layer-dependent electrostatic potential $\propto eEd$ (The sizes of spin splitting can be calculated by eEd). Using $E=0.02\text{V}/\text{\AA}$ as an example, the Berry curvatures calculations in Fig.3 (c) and (d) show that the Berry curvatures of spin-up and spin-down channels around Y_1 and X_1 valleys are opposite. In the presence of a longitudinal in-plane electric field E_{\parallel} , the spin-up electrons from only X_1 valley accumulate along one side of bottom Fe layer, which leads to the layer-locked anomalous valley Hall effect of Fig.1 (d). When the direction of electric field is reversed, the spin-down electrons from only X_1 valley accumulate along the other side of top Fe layer, leading to a electric field-effect induced sign reversal of the AVHE previously predicted in FV-FM system [54].

Valley-polarized quantum spin Hall insulator.-

The Fe₂BrMgP has been predicted to be an AFM quantum spin Hall insulator (QSHI) with high spin Chern numbers, as confirmed by the gapless edge states and the topological invariant spin Chern numbers (C_s) [51]. By applying uniaxial strain and electric field simultaneously, the VQSHI can be achieved in Fe₂BrMgP, which combines AVHE and QSHE in one material, providing a path towards integrating valleytronics, topological quantum effects and spintronics in a single system. To confirm this aspect, for Fe₂BrMgP with $a/a_0=1.04$ at $E=+0.02\text{V}/\text{\AA}$, the edge states along the [100] direction and the evolution of the Wannier charge centers (WCCs) along k_y are plotted in Fig.6. Based on the evolution of WCCs, the spin Chern number $|C_s|$ is 2, which is further determined by two pairs of gapless edge states with opposite chiralities appearing in the bulk gap. Therefore, VQSHI can indeed be realized in Fe₂BrMgP.

Conclusion.— In summary, we propose a paradigm for achieving anomalous valley Hall effect in AFM tetragonal monolayers by external field and strain engineering. The proposed concept is confirmed by a prototype monolayer Fe₂BrMgP using first-principles calculations. Uniaxial strain induces valley polarization by breaking C_4 symmetry, and an out-of-plane electric field gives rise to spin splitting via layer-dependent electrostatic potential. The concept of VQSHI is demonstrated, which is similar to VQAH. Our analysis can be readily extended to the broader family of Fe₂XY ($X=\text{or}\neq Y=\text{Cl, Br and I}$) and Li₂Fe₂XY ($X=\text{or}\neq Y=\text{S, Se and Te}$) bilayers as they share the same Fe-dominated low-energy states as Fe₂BrMgP. Our results reveal a route towards energy-saving and fast-operating spintronic-valleytronic devices based on 2D antiferromagnetic materials.

ACKNOWLEDGMENTS

We are grateful to Shanxi Supercomputing Center of China, and the calculations were performed on TianHe-2. Y.S.A. is supported by the Singapore Ministry of Education Academic Research Fund Tier 2 (Award No. MOE-T2EP50221-0019).

-
- [1] J. R. Schaibley, H. Yu, G. Clark, P. Rivera, J. S. Ross, K. L. Seyler, W. Yao and X. Xu, *Nat. Rev. Mater.* **1**, 16055 (2016).
 - [2] G. Pacchioni, *Nat. Rev. Mater.* **5**, 480 (2020).
 - [3] S. A. Vitale, D. Nezich, J. O. Varghese, P. Kim, N. Gedik, P. Jarillo-Herrero, D. Xiao and M. Rothschild, *Small* **14**, 1801483 (2018).
 - [4] D. Xiao, M. C. Chang and Q. Niu, *Rev. Mod. Phys.* **82**, 1959 (2010).
 - [5] Y. S. Ang, S. A. Yang, C. Zhang, Z. Ma, and L. K. Ang, *Phys. Rev. B* **96**, 245410 (2017).
 - [6] K. E. J. Goh, C. P. Y. Wong, and T. Wang, *Valleytronics in 2D materials* (World Scientific, 2023).
 - [7] L. L. Tao, A. Naemi, and E. Y. Tsymal, *Phys. Rev. Appl.* **13**, 054043 (2020).
 - [8] A. Srivastava, M. Sidler, A. V. Allain, D. S. Lembke, A. Kis and A. Imamoglu, *Nat. Phys.* **11**, 141 (2015).
 - [9] K. F. Mak, K. He, J. Shan and T. F. Heinz, *Nat. Nanotechnol.* **7**, 494 (2012).
 - [10] H. Zeng, J. Dai, W. Yao, D. Xiao, and X. Cui, *Nat. Nanotechnol.* **7**, 490 (2012).
 - [11] M. Zeng, Y. Xiao, J. Liu, K. Yang and L. Fu, *Chem. Rev.* **118**, 6236 (2018).
 - [12] C. Zhao, T. Norden, P. Zhang, P. Zhao, Y. Cheng, F.

- Sun, J. P. Parry, P. Taheri, J. Wang, Y. Yang, T. Scrace, K. Kang, S. Yang, G. Miao, R. Sabirianov, G. Kioseoglou, W. Huang, A. Petrou and H. Zeng, *Nat. Nanotechnol.* **12**, 757 (2017).
- [13] D. MacNeill, C. Heikes, K. F. Mak, Z. Anderson, A. Kormányos, V. Zólyomi, J. Park and D. C. Ralph, *Phys. Rev. Lett.* **114**, 037401 (2015).
- [14] W. Y. Tong, S. J. Gong, X. Wan and C. G. Duan, *Nat. Commun.* **7**, 13612 (2016).
- [15] J. Zheng, Y. Zhao, Y. Tan, Z. Guan, N. Zhong, F. Yue, P. Xiang and C. G. Duan, *J. Appl. Phys.* **132**, 120902 (2022).
- [16] X. Hu, *Adv. Mater.* **24**, 294 (2012).
- [17] T. Jungwirth, J. Sinova, A. Manchon, X. Marti, J. Wunderlich and C. Felser, *Nat. Phys.* **14**, 200 (2018).
- [18] W. Du, R. Peng, Z. He, Y. Dai, B. Huang and Y. Ma, *npj 2D Mater. Appl.* **6**, 11 (2022).
- [19] X. Xu, Z. He, Y. Dai, B. Huang and Y. Ma *Phys. Rev. B* **104**, 205430 (2021).
- [20] W. Zhou, G. Zheng, A. Li, D. Zhang and F. Ouyang, *Phys. Rev. B* **107**, 035139 (2023).
- [21] X. Li, T. Cao, Q. Niu, J. Shi and J. Feng, *PNAS*, **110**, 3738 (2013).
- [22] T. Zhao, S. Xing, J. Zhou, N. Miao and Z. Sun, *Journal of Materiomics* (2023), doi: <https://doi.org/10.1016/j.jmat.2023.10.008>.
- [23] C. Nayak, S. H. Simon, A. Stern, M. Freedman and S. Das Sarma, *Rev. Mod. Phys.* **80**, 1083 (2008).
- [24] M. Z. Hasan and C. L. Kane, *Rev. Mod. Phys.* **82**, 3045 (2010).
- [25] X.-L. Qi and S.-C. Zhang, *Rev. Mod. Phys.* **83**, 1057 (2011).
- [26] F. D. M. Haldane, *Phys. Rev. Lett.* **61**, 2015 (1988).
- [27] C. Z. Chang, J. Zhang, X. Feng, J. Shen, Z. Zhang, M. Guo, K. Li, Y. Ou, P. Wei, L. Wang, Z. Ji, Y. Feng, S. Ji, X. Chen, J. Jia, X. Dai, Z. Fang, S. C. Zhang, K. He, Y. Wang, L. Lu, X. C. Ma and Q. K. Xue, *Science* **340**, 167 (2013).
- [28] Y. Deng, Y. Yu, M. Z. Shi, Z. Guo, Z. Xu, J. Wang, X. H. Chen and Y. Zhang, *Science* **367**, 895 (2020).
- [29] M. Bora, S. K. Behera, P. Samal and P. Deb, *Phys. Rev. B* **105**, 235422 (2022).
- [30] M. Vila, J. H. Garcia and S. Roche, *Phys. Rev. B* **104**, L161113 (2021).
- [31] H. Pan, Z. Li, C. C. Liu, G. Zhu, Z. Qiao and Y. Yao, *Phys. Rev. Lett.* **112**, 106802 (2014).
- [32] J. Zhou, Q. Sun and P. Jena, *Phys. Rev. Lett.* **119**, 046403 (2017).
- [33] F. Zhan, Z. Ning, L.Y. Gan, B. Zheng, J. Fan and R. Wang, *Phys. Rev. B* **105**, L081115 (2022)
- [34] X D. Zhu, Y. Q. Chen, Z. Liu, Y. L. Han and Z. H. Qiao, *Front. Phys.* **18**, 23302 (2023)
- [35] Q. Sui, J. Zhang, S. Jin, Y. Xia and G. Li, *Chin. Phys. Lett.* **37**, 097301 (2020).
- [36] Z. Liu, Y. Han, Y. Ren, Q. Niu and Z. Qiao, *Phys. Rev. B* **104**, L121403 (2021).
- [37] S. D. Guo, Y. L. Tao, W. Q. Mu and B. G. Liu, *Front. Phys.* **18**, 33304 (2023).
- [38] S. Li, Q. Q. Wang, C. M. Zhang, P. Guo and S. A. Yang, *Phys. Rev. B* **104**, 085149 (2021).
- [39] W. Y. Pan, *Phys. Rev. B* **106**, 125122 (2022).
- [40] S. D. Guo, W.-Q. Mu, J.-H. Wang, Y.-X. Yang, B. Wang and Y.-S. Ang, *Phys. Rev. B* **106**, 064416 (2022).
- [41] K. Sheng, B. K. Zhang, H. K. Yuan and Z. Y. Wang, *Phys. Rev. B* **105**, 195312 (2022).
- [42] P. Liu, S. Liu, M. Jia, H. B. Yin, G. Zhang, F. Ren B. Wang and C. Liu, *Appl. Phys. Lett.* **121**, 063103 (2022).
- [43] S. D. Guo, G. Wang, and Y. S. Ang, *Appl. Phys. Lett.* **123**, 173102 (2023).
- [44] S. D. Guo and Y. S. Ang, *Phys. Rev. B* **108**, L180403 (2023).
- [45] Q. L. Sun, Y. D. Ma and N. Kioussis, *Mater. Horiz.* **7**, 2071 (2020).
- [46] Y. Li, J. H. Li, Y. Li, M. Ye, F. W. Zheng, Z. T. Zhang, J. H. Fu, W. H. Duan and Y. Xu, *Phys. Rev. Lett.* **125**, 086401 (2020).
- [47] S. D. Guo, W. Q. Mu, X. B. Xiao and B. G. Liu, *Nanoscale* **13**, 12956 (2021).
- [48] J. Y. Li, Q. S. Yao, L. Wu, Z. X. Hu, B. Y. Gao, X. G. Wan and Q. H. Liu, *Nat. Commun.* **13**, 919 (2022).
- [49] S. D. Guo, Y. T. Zhu, J. L. Xin and B. G. Liu, *J. Mater. Chem. C* **10**, 8381 (2022).
- [50] S. D. Guo, W. Q. Mu, M. Y. Yin, Y. C. Li and W. C. Ren, *J. Phys. D: Appl. Phys.* **54**, 505006 (2021).
- [51] Y. Xue, W. Xu, B. Zhao, J. Zhang and Z. Yang, *Phys. Rev. B* **108**, 075138 (2023).
- [52] K. N. Duerloo, M. T. Ong and E. J. Reed, *J. Phys. Chem. Lett.* **3**, 2871 (2012).
- [53] C. Lee, X. g Wei, J. W. Kysar and J. Hone, *Science* **321**, 385 (2008).
- [54] X. Zhou, R.-W. Zhang, Z. Zhang, W. Feng, Y. Mokrousov, and Y. Yao, *npj Comput. Mater.* **7**, 160 (2021).